# Three Dimensional Bright Spatial Soliton Collision and Fusion in a Saturable Nonlinear Medium

Vladimir Tikhonenko, Jason Christou, and Barry Luther-Davies
*Laser Physics Centre, Research School of Physical Sciences and Engineering, Australian National University, Canberra ACT 0200, Australia*
(Received 28 September 1995)

We report experiments showing of the attraction and novel fusion behavior of 3D bright spatial solitons, formed by modulation instability of an optical vortex in a saturable self-focusing medium.

PACS numbers: 42.65.Tg, 03.40.Kf, 42.65.Jx

The physical nature of self-focusing and self-trapping resulting from the optical Kerr effect has been understood since the 1960s [1]. It is also known that a self-trapped beam propagating in three spatial dimensions through an ideal Kerr medium is unstable [2,3]. Saturation of the Kerr response [4], however, stabilizes the process and allows the formation of stationary solitary waves [5], referred to as 3D bright spatial solitons. Such solitons are expected to interact (attract, repel, etc.) in a way analogous to the more widely studied case of 2D bright spatial solitons [6,7]. Our aim was to investigate the interaction between in-phase 3D bright spatial solitons, experimentally, as they propagated through a saturable self-focusing medium. We were able to observe a number of novel phenomena including attraction and fusion [8] of the solitons and behavior arising from conservation of angular momentum for the vortex field used to generate the solitons. The experimental observations and numerical simulations were in excellent agreement.

To generate a pair of in-phase bright spatial solitons we used the method described in Ref. [9] but imposed a doubly, rather than a singly, charged optical vortex [10] on the axis of a slightly elliptical laser beam. After linear propagation this beam developed the double-lobed annular structure shown in Fig. 1(a) with the vortex (which in fact decays into a closely separated pair of singly charged vortices) responsible for the near on-axis intensity zero. When this beam propagates through a self-focusing medium it is susceptible to breakup via modulational instability, into two soliton-like spots on diametrically opposite sides of the beam axis [11]. The initial intensity distribution, which varies slightly in the azimuthal direction, strongly seeds this decay. Because the solitons so formed inherit the local phase of the original beam, they are in phase whenever the vortex has even charge. By increasing the nonlinear propagation distance, one can expect features reflecting the interaction between solitonlike beams to appear in the transverse intensity distribution.

Experimentally it was impractical to vary the propagation length in the medium; our observations were of the intensity pattern at the output of a medium whose nonlinearity could be varied. The nonlinear medium was low pressure ($10^{11-12}$ cm$^{-3}$) rubidium vapor contained within a 200 mm long glass cell, with no buffer gas, in a double chamber oven. The input beam was generated by a cw Ti:sapphire laser tuned near the Rb $D_2$ resonance line at 780 nm. Enhancement of the self-focusing nonlinearity could be obtained by tuning relative to the $5S_{1/2}(F = 3) \rightarrow 5P_{3/2}(F = 4)$ hyperfine transition. At these low pressures collisional broadening was negligible and the Doppler-limited linewidth of the working resonance was $\approx$0.75 GHz (at 100 °C). The laser was detuned from 1.5 to 0.5 GHz on the high frequency side of the transition, providing the maximum range of focusing nonlinearity for the least absorption.

The vortex was created by passing the laser beam through a diffracting phase mask. The mask was produced, using lithographic techniques, from a computer-generated binary pattern representing the interference between a plane wave and a wave containing a doubly charged optical vortex. The background fringe frequency was 130 cm$^{-1}$ and the diffraction efficiency was $\approx$80% (total power into the two first order diffracted beams). After demagnification, the vortex beam was imaged onto the input of the cell with a beam diameter $\sim$0.25 mm. Further details of the experimental arrangement can be found in Ref. [9]. The patterns at the output of the cell were viewed with a cooled charge coupled device camera and recorded using a frame grabber. It was also possible to view the fluorescence from the Rb vapor through side windows along the cell.

Figure 1 shows the intensity pattern at the output of the cell with increasing nonlinearity. The sequence shows two distinct stages in the evolution of the spatial intensity patterns. In the first stage [Figs. 1(a)–1(c)], only two local intensity maxima were observed. These three pictures demonstrate the breakup in the azimuthal direction due to modulational instability of the annular beam [12] to form a pair of solitonlike beams. As the "solitons" form they start to rotate about their common axis and attract each other, the rotation rate increasing as they approach. The sense of rotation was clockwise for the $+2$ vortex and anticlockwise when the $-2$ vortex was used. As detuning was further reduced, a second stage in the evolution began. This was characterized by the appearance of an additional on-axis intensity maximum [Fig. 1(d)].

 0031-9007/96/76(15)/2698(4)$10.00 

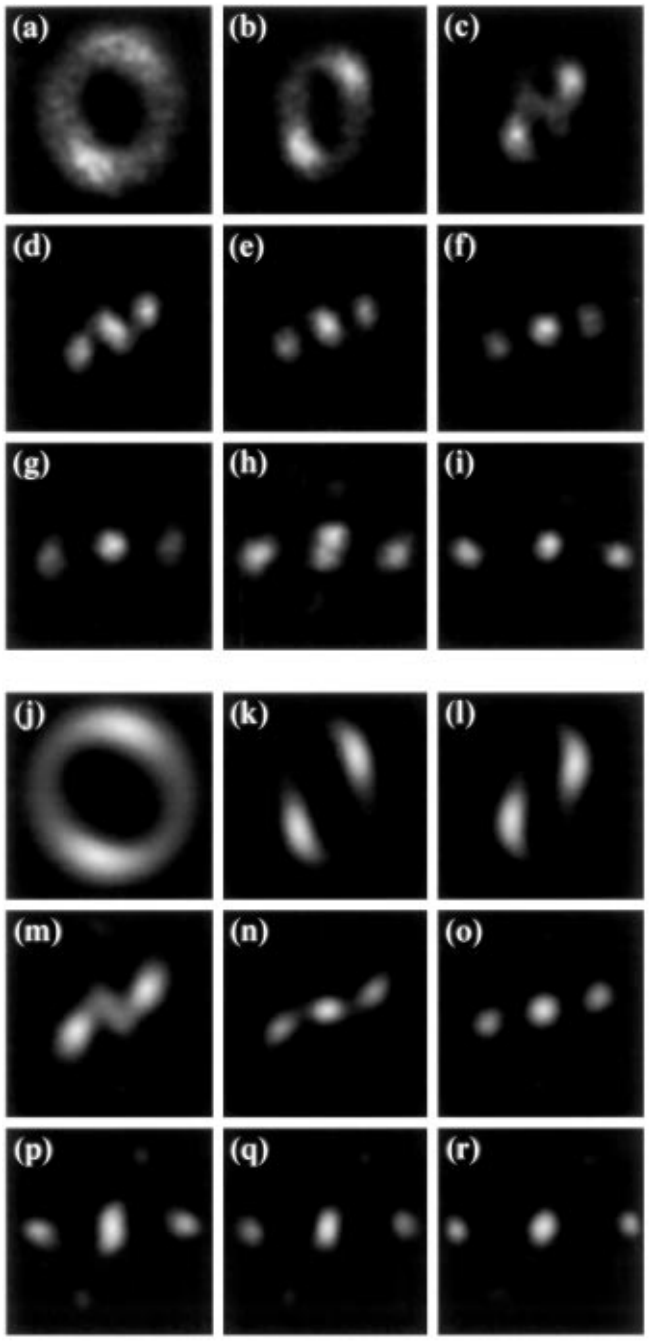


FIG. 1. Comparison of experimental results and simulation. Experimental beam profiles at the output window of the cell are shown in the upper set of pictures for detunings equal to (a) 30 (b) 27, (c) 26, (d) 25, (e) 24, (f) 23, (g) 21, (h) 20, (i) 16 with each $\times\Delta\nu_L$ (laser linewidth $\Delta\nu_L \approx 40$ MHz). The window size was 0.8 mm $\times$ 0.8 mm. Calculated beam profiles are shown in the lower set of pictures for concentrations, $N_{\mathrm{Rb}}$, equal to (j) 1.1, (k) 1.5, (l) 1.9, (m) 2.3, (n) 2.7, (n) 3.1, (o) 3.1, (p) 3.5, (q) 3.9, (r) 5.2 each in units of $\times 10^{11}$ cm$^{-3}$.

The two outer filaments began to fuse as they reached their point of closest approach, transferring energy into a central lobe [Figs. 1(d)–Fig. 1(f)]. Rotation of the outer filaments continued in the clockwise sense, but as they fused their radial motion reversed, taking them away from the axis. The central filament, while remaining on-axis, displayed a nonstationary profile as nonlinearity increased further, at times appearing to be composed of two very closely spaced individual filaments [Fig. 1(h)]. Eventually, both the rotation and outward motion of the outer filaments tended to saturate, yielding an approximately stable output pattern [Fig. 1(g)–1(i)], although total intensity decayed at higher nonlinearities due to increased absorption near the transition frequency.

Propagation behavior of the vortex was observed through the side window of the oven. For output profiles containing only two maxima, this view showed the presence of only two filaments within the medium, except during the first 3 cm of propagation, where they were not yet formed. When three maxima were observed at the output window, the side views showed that the input beam first formed two filaments [Fig. 2(a)] with the third filament appearing at longer propagation distances [Fig. 2(b)].

It is worth noting that the general behavior reported above was not critically dependent on any particular experimental parameter. Similar results could therefore be obtained by varying cell temperature, or laser power to alter the effective nonlinearity of the medium.

Numerical simulations were carried out for comparison with these experiments using the beam propagation method. The slowly varying envelope of the electric field at the cell input took the form $A(x, y, z = 0) = A_0 \exp[-(x^2/w_x^2 + y^2/w_y^2) + i2\tan^{-1}(y/x)]$, with the intensity ($I = |A|^2$) dependent dielectric constant of the medium approximated as $\varepsilon(I) = n_0^2 + 2n_0 \times [n_{\mathrm{n1}}(I) - i\gamma(I)/k_0]$, $\gamma$ being the absorption coefficient and $n_{\mathrm{n1}}$ the nonlinear refractive index. Estimates of real and imaginary parts of the dielectric constant were based on a two-level atom model with inhomogeneously broadened transitions in the presence of strong hole burning [13]. The values obtained in this way have a complicated form, depending on both detuning ($\Delta\nu_1$), intensity, and vapor concentration ($N_{\mathrm{Rb}}$). The calculated dependencies of the dielectric constant were interpolated by simpler fitting functions, with the best fit obtained for a nonlinear index,

$$n_{\mathrm{n1}}(\Delta\nu_1, N_{\mathrm{Rb}}, I) \approx \frac{n_s(\Delta\nu_1, N_{\mathrm{Rb}})I}{1 + I/I_{s1}(\Delta\nu_1)} \qquad (1a)$$

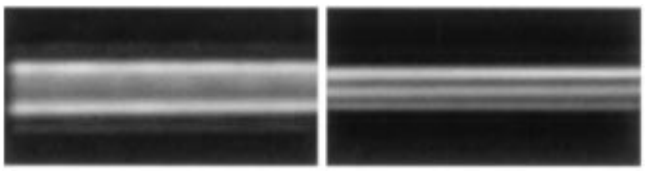


FIG. 2. Side window observations of beam configuration. Images were taken at distances of (a) 7 cm and (b) 20 cm along the cell. Image size = 5 mm $\times$ 20 mm, detuning $= 17\Delta\nu_L$.

and an absorption,

$$\gamma(\Delta\nu_1, N_{\mathrm{Rb}}, I) \approx \frac{\gamma_s(\Delta\nu_1, N_{\mathrm{Rb}})}{\sqrt{1 + I/I_{s2}(\Delta\nu_1)}}, \qquad (1b)$$

where $n_s$ is the saturated Kerr coefficient and $\gamma_s$ is the low intensity absorption coefficient. The following parameter set was used for simulations: $I_{s1} = 5.5$ W/cm$^2$; $I_{s2} = 0.01$ W/cm$^2$; $n_s = 0.9 \times 10^{-17} N_{\mathrm{Rb}}$ cm$^2$/W; $\gamma_s = 0.2 \times 10^{-11} N_{\mathrm{Rb}}$ cm$^{-1}$, with $N_{\mathrm{Rb}}$ in cm$^{-3}$.

Results from a sequence of simulations for increasing nonlinearity at a fixed propagation distance of 20 cm are shown in Figs. 1(j)–1(r). The power at the input was 25 mW ($A_0^2 = 16$ W/cm$^2$), with the input radii given by $w_x = 0.34$ mm and $w_y = 0.27$ mm. Model parameters were taken from those listed above, using $N_{\mathrm{Rb}}$ values ranging from $1.1 \times 10^{11}$ to $5.2 \times 10^{11}$ cm$^{-3}$. The values of $n_s$ and $\gamma_s$ calculated for these concentrations cover the same values obtained experimentally by detuning, though it was more convenient in experiment to range over detuning rather than concentration, given the similar behavior of output profiles for the two cases. Good agreement between simulation and experiment shows that the model for nonlinearity fits well with the actual response of the medium. All features of the behavior described above were observed in the calculated profiles. There is slight disagreement in that splitting of the central peak was not resolved, although oscillatory changes in shape, were apparent. Varying the simulation parameters over a feasible experimental range did not affect the general behavior of the output beam profiles.

The numerical simulations allowed investigation of beam dynamics during propagation through the medium where, experimentally, this could be monitored only through side windows. The calculated propagation dynamics of the field is shown in Fig. 3. Two filaments form from the elliptical ring structure of the beam after about 7 cm propagation, as was seen in experimental side views. A collision between this pair of filaments is responsible for generation of the third, central filament, seen at longer propagation distances, in agreement with Fig. 2.

In both experiment and simulations only partial fusion of the soliton pair was observed. There are reasons why complete fusion might not occur when bright solitons are created from a beam containing an optical vortex because of the need to conserve "angular momentum" for the beam. The expression for the angular momentum [14],

$$L_z = \frac{i}{2} \int_{-\infty}^{\infty} \int_{-\infty}^{\infty} \left[ x\left( A \frac{\partial A^*}{\partial y} - A^* \frac{\partial A}{\partial y} \right) - y\left( A \frac{\partial A^*}{\partial x} - A^* \frac{\partial A}{\partial x} \right) \right] dx\, dy\,, \qquad (2)$$

arises from rotational invariance of the field equations [15]. For the incident optical vortex used in these experiments, this integral is nonzero. Solitons which are formed from vortex breakup must conserve angular momentum at all propagation distances, at least when absorption is neglected.

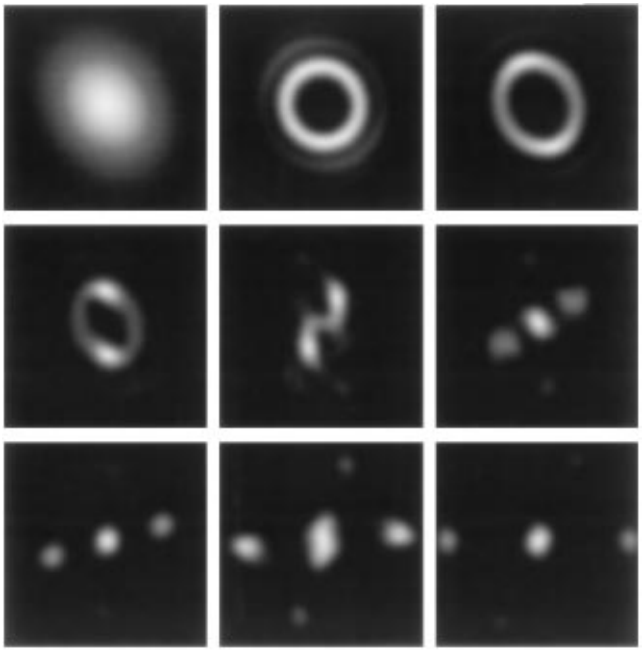

FIG. 3. Propagation dynamics of calculated beam profile. From top left to bottom right by row, propagation distance = 0, 2.5, 5, 7.5, 10, 12.5, 15, 17.5, and 20 cm.

If it is assumed that the solitons approximately retain their shape and are permitted to move along some nearly longitudinal path, then it is possible to obtain a more transparent form for the angular momentum conservation law. The envelope for such a soliton has an approximate form [16]:

$$A(\mathbf{r}_\perp, z) \approx u(\mathbf{r}_\perp - \mathbf{r}_0(z)) \exp\left[ ik_0 n_0 \frac{\partial \mathbf{r}_0}{\partial z} \cdot \mathbf{r}_\perp \right] \times \exp[i\beta z], \qquad (3)$$

where $u$ is the shape of the soliton, $\mathbf{r}_\perp = [x, y]$ is the transverse coordinate, $\mathbf{r}_0 = [x_0(z), y_0(z)]$ is the position of the profile, $\beta$ is a propagation constant, and the transverse phase variation simply acts to make the planes of constant phase normal to the soliton's direction of propagation. To ensure a slowly varying envelope $A$, with respect to the carrier $\exp[-ik_0 n_0 z]$, the parameters should satisfy $\|\partial \mathbf{r}_0/\partial z\|, \beta/k_0 n_0 \ll 1$. Substituting (3) into (2), a simple form for the conservation law is obtained, converting $\mathbf{r}_0$ to its polar representation:

$$L_z = k_0 n_0 P_0 r_0^2 \frac{\partial \theta_0}{\partial z}, \qquad (4)$$

where $P_0$ is the beam power. This is the same form as mechanical angular momentum for a particle of "mass" $P_0$, with time substituted for propagation $k_0 n_0 z$. For fields consisting of well separated solitons, the total angular momentum is the sum of the individual angular

momenta. The use of the vortex as the incident field means that this sum was nonzero in our experiments.

Calculations of the angular momentum were carried out for propagation simulations akin to Fig. 3. The angular momentum and power versus propagation distance for $n_s = 5 \times 10^{-6}$ cm$^2$/W and neglecting absorption are shown in Fig. 4. The beam power slowly decreases due to spread of energy into regions outside the integration window. Note that not all of the energy in the initial beam ends up in solitons. Some energy contributes to a low intensity "radiation" field which spreads, by diffraction, past the integration area in our numerical grid. The important feature of this figure is that as the solitons move outside the integration window the angular momentum drops to zero in spite of the fact that ~40% of the total beam power remains within the integration window in the central lobe. Almost all the angular momentum of the beam is carried by the outer beams. Hence as power flows from them to the central spot they must move outwards and away from the axis, along some nonradial path, $\partial\theta_0/\partial z \neq 0$, to conserve angular momentum. The inclusion of absorption has negligible effect on these results.

To conclude, we have studied experimentally the breakup of a beam containing a doubly charged optical vortex in a saturable self-focusing medium. By seeding the modulation instability the input beam transforms into a pair of in-phase soliton-like beams which attract and fuse as anticipated by earlier numerical simulations. The beam behavior is accurately simulated by our computations which model the medium nonlinearity using simple saturating functions. Complete fusion of the soliton pair appears impossible in this experiment because of the need to conserve angular momentum of the beam. According to our numerics, the central spot created by fusion contains negligible angular momentum. As a result the fusing pair flies away from the beam axis to conserve angular momentum as their power drops.

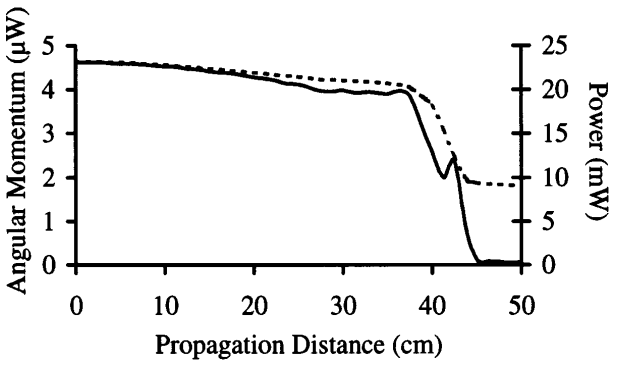


FIG. 4. Angular momentum and power integrals vs propagation distance (without absorption). Solid curve represents angular momentum, dashed curve indicates power. The window for integration was 1.5 mm × 1.5 mm inside a calculation window of 3 mm × 3 mm.

Demonstration of fusion is not without practical importance. Logic and switching mechanisms employing soliton collision and fusion have been proposed whereby the fused soliton is present at some position only if both input soliton signals were present. Interaction forces can also be interesting in that a variety of trajectories may be traced out by a pair of solitons depending on the balance of the interaction with the "centrifugal forces." For instance a bound states exist [17], where the soliton pair spirals in fixed orbit, which is likely to provide a striking experimental example of beam interaction in the nonlinear medium. Appropriate variants on the vortex propagation and soliton interaction experiment shown here are currently being investigated.

The partial support of the Australian Photonics Cooperative Research Centre is gratefully acknowledged.

[1] R. Y. Chiao, E. Garmire, and C. H. Townes, Phys. Rev. Lett. **13**, 479 (1964); P. L. Kelley, Phys. Rev. Lett. **15**, 1005 (1965); D. Grishkowsky, Phys. Rev. Lett. **24**, 866 (1970); J. E. Bjorkholm and A. Ashkin, Phys. Rev. Lett. **32**, 129 (1974); K. Konar and A. Sengputa, J. Opt. Soc. Am. B **11**, 1644 (1994), and references therein.

[2] Y. Silberberg, Opt. Lett. **15**, 1282 (1990).

[3] M. Desaix, D. Anderson, and M. Lisak, J. Opt. Soc. Am. B **8**, 2082 (1991).

[4] V. S. Butylkin, A. E. Kaplan, Yu. G. Khronopulo, and E. I. Yakubovic, *Resonant Nonlinear Interactions of Light with Matter* (Springer-Verlag, Berlin, 1989).

[5] A. W. Snyder, D. J. Mitchell, L. Poladian, and F. Ladouceur, Opt. Lett. **16**, 21 (1991).

[6] F. Reynaud and A. Barthelemy, Europhys. Lett. **12**, 401 (1990).

[7] J. P. Gordon, Opt. Lett. **8**, 596 (1983).

[8] A. W. Snyder and A. P. Sheppard, Opt. Lett. **18**, 482 (1992).

[9] V. Tikhonenko, J. Christou, and B. Luther-Davies, J. Opt. Soc. Am. **12**, 2046 (1995).

[10] I. V. Basistiy, V. Yu. Buzhenov, M. S. Soskin, and M. V. Vasnetsov, Opt. Commun. **94**, 469 (1992).

[11] J. Atai, Y. Chen, and J. M. Soto-Crespo, Phys. Rev. A **49**, 3170 (1994).

[12] J. M. Soto-Crespo, D. R. Heatley, E. M. Wright, and N. N. Akhmediev, Phys. Rev. A **44**, 636 (1991).

[13] D. H. Close, Phys. Rev. **153**, 360 (1967).

[14] Ignoring absorption, the Lagrangian density for the slowly varying scalar field is invariant with respect to coordinate rotations. Using the prescription given in Chap. 7, Sec. 38 of Ref. [15], the conserved quantity associated with this invariance is given by Eq. (6).

[15] I. M. Gelfand and S. V. Fomin, *Calculus of Variations* (Prentice-Hall, Englewood Cliffs, NJ, 1963).

[16] D. J. Mitchell, A. W. Snyder, and L. Poladian, Electron. Lett. **27**, 848 (1991).

[17] L. Poladian, A. W. Snyder, and D. J. Mitchell, Opt. Commun. **85**, 59 (1991).